Sustainable Energy & Fuels

ROYAL SOCIETY OF CHEMISTRY

PAPER

View Article Online
View Journal | View Issue

Cite this: *Sustainable Energy Fuels*, 2020, **4**, 5674

Increasing dimethyl ether production from biomass-derived syngas *via* sorption enhanced dimethyl ether synthesis

Dalia Liuzzi,[a] Cristina Peinado,[a] Miguel A. Peña,[a] Jasper van Kampen,[b] Jurriaan Boon[b] and Sergio Rojas *[a]

The direct synthesis of dimethyl ether (DME) from biomass-derived syngas is a topic of great interest in the field of biofuels. The process takes place in one reactor combining two catalytic functions, $Cu/ZnO/Al_2O_3$ (CZA) for the synthesis of methanol and an acid catalyst (typically γ-Al_2O_3) for methanol dehydration to DME. However, the catalytic performance of those catalysts is negatively affected by the high CO_2/CO ratio in the bio-syngas, resulting in low methanol and DME production rates. In this work, we show that promoters such as zirconium and gallium oxides increase the CO fraction in the syngas. However, the production of H_2O is also increased, leading to the deactivation of both CZA and γ-Al_2O_3. The addition of a water sorbent (zeolite 3A) in the reaction medium alleviates the detrimental effect of H_2O in the direct synthesis of DME from CO_2-rich syngas. Thus, DME production over the CZA/γ-Al_2O_3 catalytic bed increases from *ca.* 8.7% to 70% when a zeolite 3A is placed in the reaction medium. In fact, carbon conversions higher than conventional equilibrium conversions are achieved. This work demonstrates that the sorption enhanced synthesis of DME is a suitable strategy to increase DME production from biomass-derived syngas.

Received 7th August 2020
Accepted 19th September 2020

DOI: 10.1039/d0se01172j

rsc.li/sustainable-energy

Introduction

The use of biomass or municipal solid waste as feedstock to produce transportation fuels and chemicals is a central policy to address environmental and oil dependence issues of today's society. The range of products that can be obtained through the different routes for biomass transformation covers from hydrogen and light hydrocarbons, to liquids fuels including diesel and kerosene.[1,2] Among those, dimethyl ether (DME) stands out as an excellent diesel substitute for ignition engines providing very low NO_x and soot in the exhaust gases.[3,4] DME production from biomass gasification is a multistep process which includes biomass gasification, syngas conditioning, production of methanol and methanol dehydration to DME among its chemical unit operations.[2,5] Usually, the syngas obtained from biomass shows a CO_2/CO ratio significantly higher than the optimum one for the synthesis of methanol, around 3–5% CO_2,[6] resulting in low once through carbon conversion.[7–9] Methanol synthesis from syngas and dehydration steps can be carried out in separate reactors, or within a single reactor.

Recently, the direct synthesis of DME from (biomass-derived) syngas or from pure CO_2 is attracting a great deal of attention.[3,4,10–15] During the direct synthesis of DME, the following reactions take place simultaneously; CO and CO_2 hydrogenation to methanol (eqn (1) and (2)), water gas shift reaction (WGS) (eqn (3)), and the dehydration of methanol to DME (eqn (4)).

$$CO + 2H_2 \leftrightarrow CH_3OH \quad (1)$$

$$CO_2 + 3H_2 \leftrightarrow CH_3OH + H_2O \quad (2)$$

$$CO + H_2O \leftrightarrow CO_2 + H_2 \quad (3)$$

$$2CH_3OH \leftrightarrow CH_3OCH_3 + H_2O \quad (4)$$

The direct synthesis of DME intends to mitigate the strong thermodynamic limitations of syngas conversion to methanol by shifting the equilibrium as methanol produced is dehydrated and thus removed from the system.[4] The direct synthesis of DME entails the use of two different catalytic phases, one for the synthesis of methanol from syngas and one for DME production. Cu–ZnO–Al_2O_3 (CZA) materials are the benchmark catalysts for the synthesis of methanol from syngas,[13,16,17] whereas acidic solids such as γ-Al_2O_3,[16,18] zeolites,[19,20] acidic oxides[21] or heteropolyacids[22–25] are the most active catalysts for the methanol dehydration to DME.

Cu^0, or more likely the Cu/ZnO interphase is considered as the active site for the methanol production.[26,27] The dependence

[a]*Grupo de Energía y Química Sostenibles, Instituto de Catálisis y Petroleoquímica, CSIC, C/Marie Curie 2, Madrid, 28049, Spain. E-mail: srojas@icp.csic.es*
[b]*Biomass and Energy Efficiency, TNO Energy Transition, P.O. Box 15, 1755 ZG Petten, The Netherlands*

of the activity on the morphology and size of copper particles[26,28] and the effect of promoters such as Mn,[20,29] Zr,[18,29,30] or Ga,[30] have been discussed thoroughly in the literature. The main carbon source for methanol, either CO or CO_2, is also a recurring topic in the literature. Although there is seemingly an agreement in that methanol is mostly produced from CO_2 (eqn (1)),[27,30,31] other authors claim that the relative hydrogenation rate of CO and CO_2 depends on the conditions and the CO_2/CO ratio of the syngas.[32,33] In part, the lack of consensus arises from the interconversion between CO and CO_2 during methanol (and direct DME) synthesis through the WGS reaction (eqn (3)). Regardless of the actual source of methanol, it is well admitted that methanol production rates from CO_2 rich syngas are slower than from CO rich ones. On the one hand, the presence of a small amount of CO_2 in the syngas is beneficial for the synthesis of methanol because it promotes the partial oxidation of metallic Cu into Cu^+, which increases methanol production rates. On the other hand, CO_2 has an inhibitory effect since it adsorbs strongly on the active sites thus poisoning the catalyst.[8,34] In addition, the presence of CO_2 in the syngas results in the production of H_2O in the reaction medium *via* the reverse water gas shift and methanol synthesis reactions (eqn (2) and (3), respectively). Water is a major source of catalyst deactivation, causing the agglomeration of the Cu particles in CZA and the deactivation of γ-Al_2O_3. Moreover, since H_2O is produced along with methanol and DME, a high partial pressures of H_2O in the reaction medium also inhibits methanol and DME production.[35] Martin *et al.* reported that the optimum CO_2 content for the methanol synthesis is 2.4 vol%.[9] Sadly, the CO_2 content of biomass-derived syngas is usually well above this optimum value.[5,36] From the catalytic point of view, it has been reported that the use of promoters such as Zr or Ga oxides increase conversion rates of rich CO_2 syngas mixtures over CZA.[37,38] However, this strategy also results in a high production of H_2O, which has to be eliminated from the reaction medium. The use of water permselective membranes or high capacity of water adsorption materials are the main technologies proposed for the *in situ* removal of water from carbon hydrogenation reactions.[39,40] Recent studies about the effect of *in situ* water removal during the synthesis of DME by placing sorbent materials in the reactor have been published.[40,41] This strategy, which is coined as sorption enhanced DME synthesis (SEDMES), aims to intensify the production of DME from syngas by shifting the equilibria towards the production of methanol and DME *via* H_2O removal. Whilst a relatively large body of work on the direct synthesis of DME is available[3,4,18,42–44] and although some theoretical models on SEDMES[45,46] and its cycling design[47] have been published, very few experimental studies on this process have been reported hitherto.[48,49] Moreover, studies conducted with CO_2-rich syngas such as that obtained from biomass gasification, which results in higher production of H_2O, are lacking in the literature.

In this work, we study the synthesis of methanol (MeS), the direct synthesis of DME (DDMES) and the sorption enhanced DME synthesis (SEDMES) using CO_2-rich syngas (CO_2/CO molar ratio of 1.9; a composition similar to that obtained from biomass-derived syngas) using CZA and γ-Al_2O_3 catalytic mixtures. With the aim to adjust the CO_2/CO syngas ratio within the reaction medium, we doped CZA with ZrO_2 and Ga_2O_3 that are known to promote the r-WGS reaction. SEDMES experiments were conducted by using zeolite 3A as H_2O adsorbent in the catalytic bed. A remarkable increase of DME production and carbon conversion was observed in the SEDMES experiments.

Experimental

Synthesis of catalysts

Copper–zinc oxide–alumina (–zirconia–gallium oxide) catalysts used in this study were synthesized by the coprecipitation technique at controlled pH and temperature. An aqueous solution of the metal nitrates ($Cu(NO_3)_2\cdot 3H_2O$; $Zn(NO_3)_2\cdot 6H_2O$; $Al(NO_3)_3\cdot 9H_2O$; $Zr(NO_3)_3\cdot xH_2O$ and $Ga(NO_3)_3\cdot xH_2O$) in the desired proportion, but maintaining a total concentration of 2 M was prepared. The solution containing the nitrate precursors and a 1.6 M solution of Na_2CO_3 were added simultaneously and dropwise to a flask containing 100 mL of Milli-Q water at 70 °C. The rate of addition was controlled to maintain a pH value of 7 for the zirconia-containing catalysts and 8 for the catalyst without zirconia, under continuous stirring. Once the addition was completed, the mixture was aged for 12 hours at room temperature. The solid obtained was recovered by filtration and rinsed with Milli-Q H_2O until the pH of the recovered liquid is *ca.* 7. The solid obtained was dried at 70 °C during 12 h, crushed and calcined under static air at 325 °C during 2.5 h. The Cu content in all catalysts is *ca.* 60% (see Table 1). The catalysts with ZrO_2 are labelled as CZAZ, and the Ga_2O_3 containing catalysts are referred to as CZAZGa. The actual Cu, ZnO, ZrO_2 and Ga_2O_3 contents in the catalysts are shown in Table 1. A commercial catalyst for methanol synthesis (CZA_comm) was used as benchmark. The zeolite sample Molsieve Type 3A (MS-1014, lot 2890000651) was purchased from UOP/ASGE (New

Table 1 Textural properties and compositions of the synthesized and commercial catalysts. Particle size (d_{Cu}), dispersion (D_{Cu}) and Cu surface area (S_{Cu})

Catalyst	Surface area, $m^2\ g^{-1}$	Pore diameter, nm	Composition (wt%)						d_{Cu}, nm	S_{Cu} (XRD), $m_{Cu}^2\ g_{cat}^{-1}$	D_{Cu}, %	S_{Cu} (chem N_2O), $m_{Cu}^2\ g_{cat}^{-1}$
			Cu	ZnO	Al_2O_3	ZrO_2	Ga_2O_3	MgO				
CZA	38	12; 36	67	29	5	—	—	—	11	41	7.8	34
CZAZ	88	6; 48	67	10	15	8	—	—	8	56	5.8	25
CZAZGa	28	13–50	63	16	13	6	1	—	9	47	—	—
CZA_comm	97	7	59	27	11	—	—	2	6	66	13.7	52

Jersey, USA). Zeolite 3A lacks of acidity. γ-Al_2O_3 (acid catalyst) was purchased as 3 mm pellets (assay >98%, Riogen NJ, USA).

Characterization

Specific surface areas and pore size distribution were determined from the N_2 adsorption–desorption isotherms collected in an Asap2020 Micromeritics at −196 °C after degasification at 140 °C.

X-ray diffractograms were obtained in a polycrystal X-ray X'Pert Pro PANalytical with a configuration θ–2θ, using CuKα radiation (wavelength of 0.15418 nm), and an Anton Paar XRK900 was used for the pre-treatment of the samples under reductive atmosphere. The size of the Cu crystallites (d_{Cu}) was calculated with the Scherrer equation (eqn (5)).

$$d_{Cu} = \frac{K\lambda}{\beta \cos \theta} \quad (5)$$

where K is the Scherrer constant, 0.94 for spherical crystals with cubic symmetry, and λ represents the wavelength of the incident radiation. β and θ are the full width at half maximum (FWHM) and the position of the diffraction peak, respectively. Based on the calculated d_{Cu}, the surface area of the reduced copper particles (S_{Cu}, $m_{Cu}{}^2\ g_{cat}{}^{-1}$) was calculated with eqn (6), in which ρ_{Cu} is the density of copper (8.92 g cm^{-3}) and Cu content is the mass fraction of copper in the catalyst.

$$S_{Cu}(XRD) = \frac{6000 \times \text{Cu content}}{\rho_{Cu}} \times d_{Cu} \quad (6)$$

The chemical composition of the catalysts was analyzed in an inducted coupled plasma-optical emission spectroscope PlasmaQuant PQ 9000 Analytik Jena, after proper digestion of the solid.

Cu dispersion and Cu surface area were determined from N_2O chemisorption. First, a temperature-programmed reduction (TPR-t) was performed by subjecting the catalyst under study to a thermal treatment between 25 to 280 °C at a rate of 2 °C min^{-1}, under a gas flow of H_2/N_2 (20/80 v/v). The temperature was decreased to 30 °C, and N_2O was flown through the reactor at 30 °C during 15 min. Once the chemisorption ended, non-chemisorbed N_2O was flushed under flowing He during 30 minutes. In this step, surface Cu species are selectively oxidized to Cu_2O. Next, a second TPR (TPR-s) was performed from 30 to 280 °C, with a heating rate of 10 °C min^{-1} under a H_2/N_2 20/80 flow. The hydrogen consumed in TPR-t stands for the totality of the copper in the catalyst. The hydrogen consumed in TPR-s accounts to the reduction of surface cupper species (Cu_2O) oxidized during the N_2O chemisorption step. Cu dispersion (D_{Cu}) was calculated from eqn (7).

$$D_{Cu}(\%) = \frac{2 \times \text{area TPR-s}}{\text{area TPR-t}} \times 100 \quad (7)$$

and the surface area of copper (S_{Cu}, in $m_{Cu}{}^2\ g_{cat}{}^{-1}$) was calculated with eqn (8).

$$S_{Cu}(\text{chem } N_2O) = a_{m,Cu} \frac{N_A D_{Cu} \text{Cu content}}{M_{Cu} \times 100} \quad (8)$$

The value of the surface area occupied by an atom of Cu in a polycrystalline surface, $a_{m,Cu}$, is 6.85 m^2 per atom of Cu. N_A is the Avogadro number and M_{Cu} is the atomic mass of Cu (63.55 g mol^{-1}). For the number of copper sites per gram of catalyst, eqn (9) was used.

$$\text{Cu sites}_{\text{cat i}} = \frac{S_{Cu}(\text{chem } N_2O) \times \rho_{S,Cu}}{N_A} \quad (9)$$

where Cu $\text{sites}_{\text{cat i}}$ is the number of copper sites in catalysts i, in moles of copper per g, and $\rho_{S,Cu}$ is de surface density of copper, which is 1.47×10^{19} atoms per m^2.

Catalytic tests

Synthesis of methanol (MeS). The catalytic tests were performed in a fixed-bed stainless-steel reactor with a diameter of 0.9 cm. The catalytic bed consisted of 200 mg of catalysts sieved at 250–300 μm fraction and diluted in SiC to avoid hot spots. The catalysts were pre-treated *in situ* in a H_2/N_2 20/80 vol current at 250 °C during 2.5 h. Afterwards, the reactor was cooled to 100 °C in N_2 and then pressurized to 25 bar with a syngas, similar to biomass-derived syngas, with a $CO/CO_2/H_2/N_2$ volumetric composition of 1/1.9/7.7/1.18 (Air Liquid), so that the M module ($[H_2–CO_2]/[CO + CO_2]$) is 2. Once reached this pressure, the reactor was heated to 270 °C and the proper flow of syngas to get a GHSV = 7500 h^{-1}. Reaction outlet gases were analysed with an on-line Varian CP-3800 gas chromatograph equipped with a Hayesep Q packed column connected to a thermal conductivity detector (TCD) and a Rtx-1 capillary column connected to a flame ionization detector (FID). N_2 was used as intern patron for the calculations of CO and CO_2 conversions. The methanol produced was calculated taking into account that it was the only product, since no other compound different to the ones in the feed was observed. The activity of each catalyst was measured for at least 5 hours. The composition of the outlet gases was analysed three times and the values reported in this work are the averaged values.

CO and CO_2 conversions were calculated as indicated in eqn (10).

$$X_i = \frac{\text{mole flow}_{i,in} - \text{mole flow}_{i,out}}{\text{mole flow}_{i,in}} \quad (10)$$

where X_i represents the conversion of compound i (CO or CO_2), and mole $\text{flow}_{i,in}$ and mole $\text{flow}_{i,out}$ are the inlet and outlet mole flows of compound i, respectively, in moles per s. For the turnover frequency numbers (TOF, in s^{-1}), eqn (11) and (12) and were used.

$$\text{Methanol production (MeS)} = \sum \text{mole low}_{i,in} \times X_i \quad (11)$$

$$\text{TOF} = \text{methanol production (MeS)}/(\text{Cu sites} \cdot g_{cat}) \quad (12)$$

Methanol production in MeS is expressed in moles per s, and g_{cat} represents the grams of catalyst loaded to the reactor. Since methanol is the only product detected, methanol production during the MeS was calculated form eqn (11).

Direct synthesis of DME (DDMES) and sorption enhanced DME synthesis (SEDMES). The metallic and acidic catalyst were

crushed to powder, mixed in a 1 : 1 weight ratio, pelletized, and finally crushed and sieved to 212–425 μm. The adsorbent zeolite 3A was also crushed and sieved to the same fraction. The catalytic bed was prepared mixing the catalysts and the zeolite in a ratio 1 : 4 (weight basis) and diluted with SiC in order to avoid the hot spots formed during the reaction.

The DDMES and SEDMES experiments were conducted on the high-pressure multi-column rig ('Spider'), with 8 reactors of 20 mm internal diameter. 5.3 g of a 1 : 1 catalyst mixture of the Cu-based and acid catalyst plus 21 g of 3A zeolite was loaded in each reactor. A flow of 90 NmL min^{-1} of simulated syngas (CO_2/CO = 2, and M = $(H_2–CO_2)/(CO + CO_2)$ = 2) was fed to each reactor at 275 °C, 25 bar. The catalytic mixture was activated under H_2/N_2 flow (20/80 v/v) at 250 °C and 1 bar during 2.5 h. Product analysis was performed by gas chromatography (GC, equipped with a TCD and a FID detector) and mass spectrometry, by monitoring the following species; hydrogen (m/z = 2), water (m/z = 18), carbon monoxide/nitrogen (m/z = 28), argon (m/z = 40), carbon dioxide (m/z = 44) and DME (m/z = 46). Traces of C_2H_4 (m/z = 28) were detected, but due to the extremely low intensity of the signal, it was not considered. C_2H_4 comes from the further dehydration of DME in presence of an acid catalyst,[50,51] so the assumption that CO and CO_2 converted only form methanol is still valid for these experiments. All experiments were performed in triplicate. The first was always discarded, the second and third reached very similar results.

The data for the SEDMES regime were those collected during the early stages of the reaction, in the transient state (*ca.* 50 minutes), when the adsorbent zeolite was still dry. The data collected once the zeolite is saturated, at steady state, represent the DDMES (after *ca.* 100 minutes). The adsorption capacity of the zeolite is regenerated *in situ*. The regeneration protocol consisted in a periodic switching to dry nitrogen, followed by decreasing the pressure to 3 bar and increasing the temperature to 400 °C. For every setting, the reaction and the regeneration were measured for every sample.

Results

Characterization

Table 1 displays the specific surface areas, pore diameters, elemental composition, and results of RXD and N_2O chemisorption of the catalysts studied in this work. As shown in Table 1, all catalysts have similar Cu loading of 60–67 wt%. CZA_comm displays the largest specific surface area in the series. Its homemade analogue (CZA) displays a lower surface area due to the lower content of Al_2O_3. The addition of ZrO_2 (CZAZ) increases the surface area of the material. On the other hand, the catalyst with gallium presents the lowest surface area of the series. The CZA_comm shows a narrow distribution of the pore sizes, while the rest of the catalysts present a bimodal distribution or a very wide range in the diameter of their pores, which are larger than in the commercial catalyst.

The X-ray diffractograms for the catalysts reduced in H_2/N_2 at 250 °C (heating rate 2 °C min^{-1}) are shown in Fig. 1. All diffractograms display the characteristic diffraction lines for metallic Cu, with peaks at 43, 50, 74° and ZnO at 32, 35, 37 and 57°. The absence of diffraction peaks for Al_2O_3, ZrO_2 or Ga_2O_3 indicates that these phases are amorphous our highly dispersed on the solid.

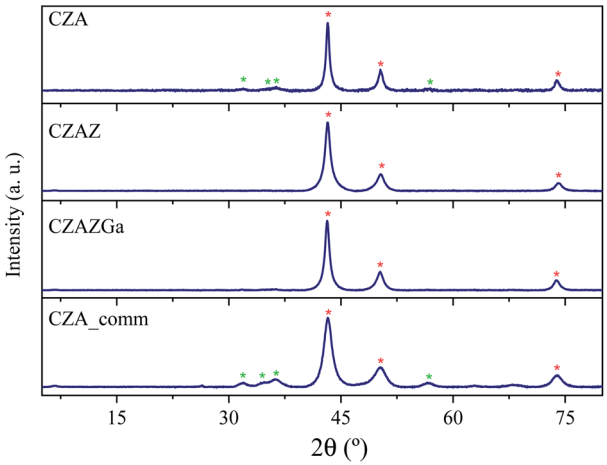

Fig. 1 X-ray diffractograms of the catalysts after reduction at 250 °C. *Cu^0, *ZnO.

Table 1 reports Cu dispersion and surface areas of the catalysts as determined from N_2O chemisorption. Sadly, it was not possible to conduct N_2O chemisorption experiment with the Ga-doped sample, CZAZGa, because Ga_2O_3 reduction overlaps with the reduction of Cu,[52] invalidating the assumption that hydrogen consumption during the experiment accounts only to the reduction of copper. Therefore, we also calculated Cu dispersion and surface area of all catalyst from the particle sizes obtained from the XRD results using eqn (5) and (6). N_2O chemisorption results reveal that CZA_comm displays the highest Cu surface area in the series, followed by CZA and CZAZ. The same trend is obtained when using the particle sizes obtained from XRD, with CZAZGa displaying the lowest Cu surface area in the series.

Catalytic activity

Three different reactions were studied in this work, namely the synthesis of methanol (MeS), the direct synthesis of DME (DDMES) and the sorption enhanced DME synthesis (SEDMES). The MeS experiments were performed as steady-state experiment, and the SEDMES and DDMES experiments were performed in a transient mode, see Fig. 2. The final steady-state conversion level, after complete saturation of the zeolite adsorbent, was taken as the DDMES experiment. The pre-breakthrough part of the experiment corresponds to the SEDMES. As an example, Fig. 2 shows the transient response for the CZA catalyst, identifying regions considered for reporting the performances of the SEDMES and DDMES modes. Although water is not removed previous to product analysis, product selectivity is reported on dry basis.

Synthesis of methanol, MeS. As shown in Fig. 3a, both CZA_comm and CZA record the highest CO and CO_2 conversions of *ca.* 7.6 and 9.9%, respectively. These conversions are

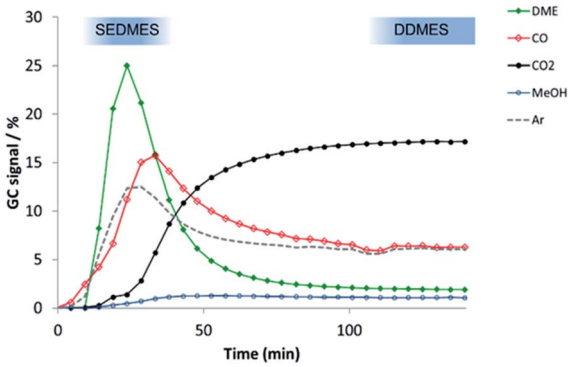

Fig. 2 Outlet compositions for DDMES and SEDMES experiment: 275 °C, 25 bar, 1080 h^{-1}, $CO_2/CO = 2$.

close to the equilibrium conversion values. Doping the catalysts with ZrO_2 decreases CO conversion to *ca.* 1.6%, without affecting CO_2 conversion. CZAZGa displays the lowest CO and CO_2 conversions in the series, with negative CO conversion of −10.6%, indicating that the content of CO in the outlet is higher than in the inlet. Negative conversion values indicate that CO is formed during the process *via* the r-WGS reaction, which is promoted by the addition of ZrO_2 and especially Ga_2O_3 to CZA. Fig. 3b shows the outlet concentrations of CO_2, CO and methanol for all catalysts. All catalysts show similar CO_2 outlet concentration around 57% mole (the equilibrium value is 58.7% mole), but the concentration of CO increases in the order CZA_comm (32.2% mole) < CZA (34.4% mole) < CZAZ (36.8% mole) < CZAZGa (39.8% mole; the equilibrium value is 32.2% mole), confirming the higher ability of CZAZ and CZAZGa for the r-WGS reaction. Methanol production is higher over the non-promoted catalysts, *i.e.*, CZA_comm (9.9% mole) and CZA (8.5% mole), decreasing over CZAZ (5.9% mole) and CZAZGa (3.1% mole) (9.1% mole at the equilibrium). A direct relationship between the outlet concentration of methanol and the Cu surface area of the catalysts obtained through N_2O chemisorption can be observed (CZA_comm > CZA > CZAZ, see Table 1). This direct relationship between methanol production and Cu surface area has been also reported by other authors.[27] In terms of TOF, a similar value of around 2×10^{-3} s^{-1} was obtained for these three catalysts. On the other hand, the activity trends shown in Fig. 3a and b reveal that even if the addition of ZrO_2 and Ga_2O_3 increases the CO/CO_2 ratio in the reactor, it does not result in higher methanol production. Martin *et al.* studied the synthesis of methanol over CZA commercial catalysts using different syngas compositions and concluded a CO_2 concentration of *ca.* 2.4% in the syngas is the optimum one for the synthesis of methanol.[9] The presence of a low amount of CO_2 suffices to form methanol and water. The H_2O formed activates the WGS reaction to produce more CO_2, which is transformed to methanol. In this way, the production and consumption of H_2O (eqn (2) and (3), respectively) are balanced in the overall process, favouring the production of methanol while avoiding catalyst deactivation *via* Cu sintering. However, when the syngas contains a high concentration of CO_2, such as that used in this work, methanol production is not optimal with CZA catalysts. In principle is it possible to adjust the CO_2/CO ratio in the syngas *via* the WGS reaction. The addition of Zr and Ga promoters to CZA catalysts improves CO_2 adsorption on the catalyst and favours the r-WGS reaction thus increasing CH_3OH production from CO_2.[18,29,30] Faen Song *et al.* found that a Zr load of approx. 3 mol% improves the dispersion of Cu and the adsorption of CO_x on the surface of the CZA, stating that higher values result in the sintering of Cu particles, and therefore a decrease of the catalyst activity.[18] W. J. Lee *et al.* studied the addition of Zr, Mg and Ga to a commercial CZA catalyst[53] and concluded that Zr favours the methanol production but lowers CO_2 conversion.

We found that doping CZA with Zr or Ga oxides promotes the r-WGS, thus increasing the CO/CO_2 ratio in the reactor. However, this effect does not lead to a higher methanol production with the doped catalysts. This can be explained by taking into account that CO_2 transformation into CO *via* the r-WGS reaction results in the production of H_2O (eqn (3)). The presence of H_2O in the reaction medium is detrimental for the production of methanol from CO_2 (eqn (2)) because it displaces the equilibrium towards the reactants. The outlet gas composition of the experiments with CZA_comm and CZA is close to the equilibrium composition (9.2% of CH_3OH). However, methanol concentration below the equilibrium value is obtained with the doped catalysts, 5.9% with CZAZ and 3.1% with CZAZ-Ga. As shown above, CZAZ and CZAZGa display the lowest ZnO content in the series (see Table 1). ZnO plays a very important role in the performance of CZA catalyst as an structural promoter of the active phase.[54–56] The presence of ZnO promotes the formation of small and stable Cu crystals on the catalyst, improves its dispersion and even promotes H_2 dissociation under conditions of deficient adsorption of H_2 on Cu particles, followed by H_2 spillover to Cu.[54] The N_2O chemisorption data reveal that the catalysts with the highest ZnO loadings (CZA_comm and CZA) display the highest Cu surface areas (see Table 1), therefore showing the highest methanol production rates. Conversely, CZAZ and CZAZGa display the lowest Cu surface areas in the series, and consequently the lower methanol production rates. In addition, it is possible that by promoting the r-WGS reaction Cu particles in the latter samples tend to agglomerate due to the excess of H_2O in the reaction medium.

Since CO_2 is the source for both methanol (eqn (2)) and CO (eqn (3)), the CH_3OH to CO ratio can be taken as a good descriptor for the preferential reaction pathway on each catalyst. Thus, high CH_3OH/CO ratios indicate that the catalyst is more active to methanol production than to the r-WGS reaction. Conversely, lower CH_3OH/CO ratios indicate that the catalyst is more active to the r-WGSR. As shown in Fig. 3a, the CH_3OH/CO-ratio decreases in the order CZA_comm > CZA > CZAZ > CZAZGa, confirming the promotional effect of ZrO_2 and Ga_2O_3 towards the r-WGS reaction.

Direct dimethyl ether synthesis, DDMES. As shown in Fig. 3c, the CO_2 and CO conversions obtained in the DDMES are higher than during the MeS with all catalysts. This observation indicates that the production of DME from methanol (eqn (4)) shifts the syngas to methanol reactions (eqn (1) and (2)) towards the formation of CH_3OH. All catalysts show similar CO_2

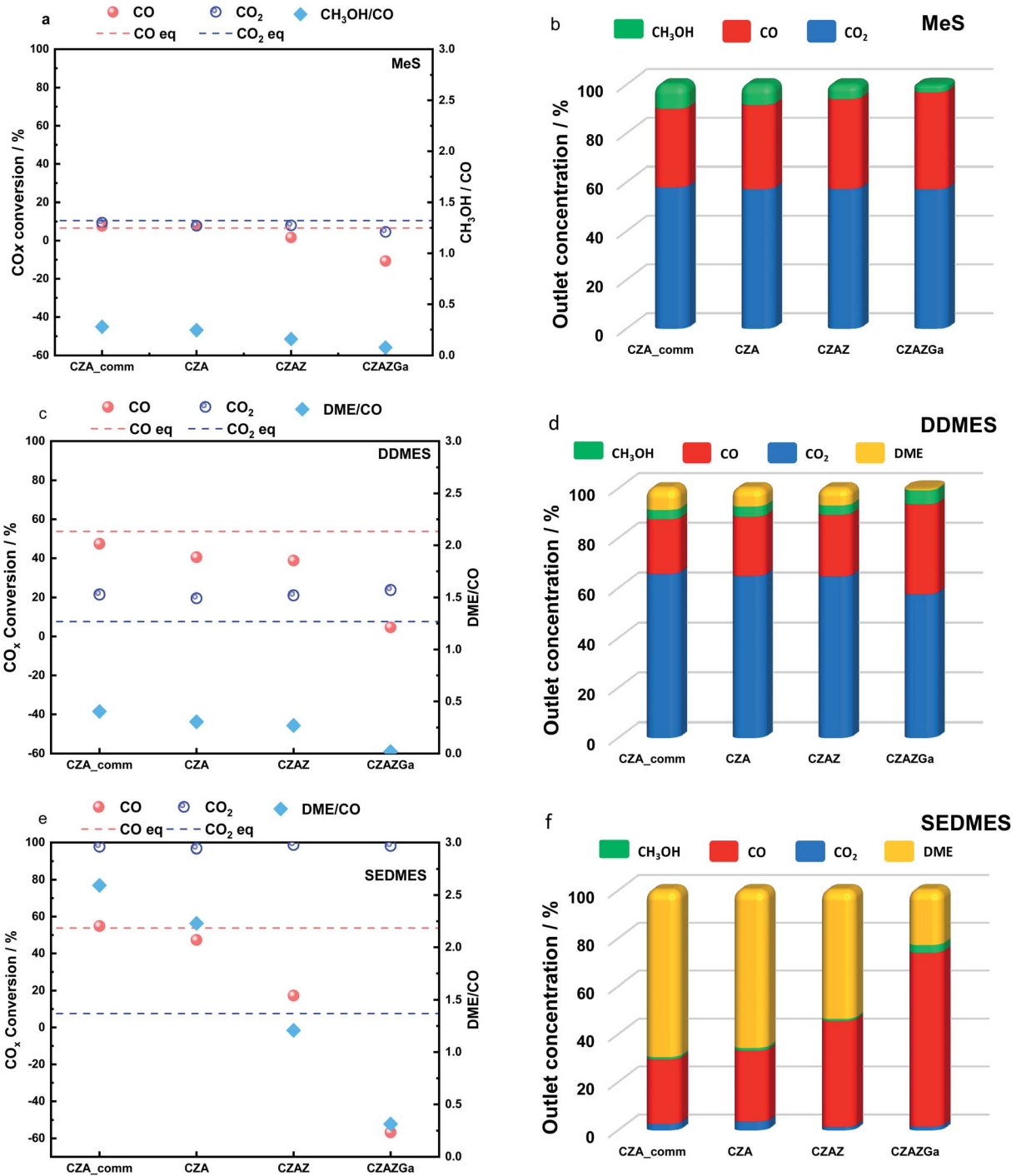

Fig. 3 CO_2 and CO conversions, CH_3OH/CO or DME/CO-ratios and outlet mole concentrations of methanol (green bar), CO (red bar), CO_2 (blue bar) and DME (yellow bar), recorded during the MeS (a and b), DDMES (c and d) and SEDMES (e and f) processes under the following conditions: DDMES and SEDMES: 275 °C, 25 bar, 1080 h^{-1}, CO_2/CO = 2; MeS: 270 °C, 25 bar, 7500 h^{-1}, CO_2/CO = 1.9.

conversions, *ca.* 20%, with CZAZGa showing a slightly higher conversion of 23%. These conversion values appear to be above the equilibrium values, but it must be noticed that the equilibrium calculations have been carried out considering only CO, CO_2, H_2, H_2O, methanol and DME in the system. As stated before, traces of C_2H_4 have been observed in both DDMES and SEDMES experiments. If ethylene is included among the products, CO and CO_2 equilibrium conversions rise to *ca.* 100% and above 50%, respectively. This effect of the presence of C_2H_4 in the reacting system on the thermodynamics can explain why the outlet concentration of CO_2 surpasses the theoretical value. On the other hand, CO conversions below the equilibrium value (54%) are observed. Again, CZA_comm shows the highest CO conversion of 47.5% followed by CZA (40.5%), CZAZ (38.8%),

and CZAZGa (4.7%). This observation contradicts previous works reporting that doping $Cu/ZnO/Al_2O_3$ catalysts with ZrO_2 increases the conversion of conversion of CO_2-containing syngas.[18,57] This feature can be due to the higher CO_2/CO ratio used in our experiments. Product selectivity is shown in Fig. 3d. As observed, methanol and DME are produced over all catalysts, with CZA_comm, CZA, and CZAZ reaching DME outlet concentrations of 8.7% mole, 7.2% mole, and 6.8% mole. Note that these values are slightly below the DME equilibrium concentration of 10.9% mole at the conditions studied in this work. CZAZGa produced a very low amount of DME, with an outlet concentration of *ca.* 0.8% mole, but shows the highest concentration of methanol of 5.7% mole *vs. ca.* 4% mole shown by the other catalysts (the equilibrium value for methanol composition is 3.8% mole). Note that the combined production of methanol and DME with CZAZGa is the lowest in the series. The lower activity towards the production of methanol and DME in the catalytic bed with CZAZGa/γ-Al_2O_3 can be explained by the very high activity of CZAZGa for the r-WGS reaction, which results in a high content of H_2O in the reaction medium, which is known to deactivate both methanol production over CZA catalysts and methanol dehydration over γ-Al_2O_3. As explained above, we used the DME/CO outlet ratio as a descriptor of the preferential reaction pathway, DME production *vs.* r-WGS reaction, with the catalysts under study during the DDMES. In line with the trend observed above for the synthesis of methanol MeS, all catalysts show a similar trend of DME/CO ratios of *ca.* between 0.4 (CZA_comm) and 0.3 (CZAZ), with CZAZGa showing the smallest ratio of 0.02, indicating a high r-WGS activity of this catalyst hence a higher CO selectivity.

Sorption enhanced DME synthesis, SEDMES. As shown in Fig. 3e, the SEDMES process results in significantly higher CO_2 conversions, *ca.* 100%, irrespectively of the catalyst under study. The CO conversions with the CZA catalysts (CZA_comm 55% and CZA 47%) are higher than in the other process, but the ones recorded with CZAZ (17%) and CZAZGa (−56%), especially the latter, are lower than the ones recorded during the DDMES and MeS. DME and methanol are produced with all catalysts. DME production is significantly higher than that obtained in the DDMES process, with outlet concentration values of 70%, 66%, 54%, and 23% mole for CZA_comm, CZA, CZAZ, and CZAZGa, respectively (Fig. 3f). All of these values are well above the aforementioned DME equilibrium concentration of 10.9% mole. The significantly higher CO and CO_2 conversions (above equilibrium) and DME production reveal the promotional effect of water removal with zeolite 3A during the direct DME synthesis from syngas.

The *in situ* removal of H_2O during the SEDMES process exacerbates the different performances between the catalysts with high activity for the production of methanol (CZA_comm and CZA) and the ones with high activity for the r-WGS reaction (CZAZ and CZAZGa). DME production is favoured over CZA and CZA_comm, indicating the higher catalytic activity of these catalysts for the reactions in which methanol and DME are produced, eqn (2) and (4), respectively. On the other hand, since the r-WGS reaction (eqn (3)) is faster than methanol production over CZAZGa, water removal promotes further the production of CO from CO_2, resulting in negative CO conversion values, which is an indication that the rate of methanol production from CO (eqn (1)) is very slow.

Finally, it is worth mentioning that the CO_2 concentration in the products in SEDMES is very low (<4%) for all catalysts, which is very important for the DME/CO_2 separation process downstream. These low CO_2 outlet concentrations suggests that the SEDMES process could be also successfully applied the direct synthesis of DME from pure CO_2/H_2 syngas.

Conclusions

In this work, we have studied the performance of a series of CZA catalysts for the synthesis of methanol and the direct synthesis of DME (using γ-Al_2O_3 as acid catalyst) from a CO_2-rich syngas, akin to that obtained from the gasification of biomass. In order to adjust the CO_2/CO ratio within the reactor, CZA has been doped with Zr and Ga oxides. This strategy allows to increase the CO/CO_2 product ratio, but it fails to increase methanol production probably due to the higher ability of the doped catalysts for the r-WGS reaction and the concomitant production of H_2O, which results in the loss of activity of the doped CZA for the production of methanol from syngas. In addition, being a reaction product, the presence of water in the reaction medium prevents the production of methanol from syngas and the production of DME from methanol. In order to remove H_2O during the direct synthesis of DME from CO_2-rich syngas we have placed an H_2O sorbent solid, zeolite 3A, in the reactor. This strategy, referred to as sorption enhanced DME synthesis (SEDMES), allows to shift the equilibria to the product side, thus resulting in higher carbon conversions and DME productions. In fact, a DME concentration of *ca.* 70%, well above the equilibrium value, was obtained with the non-doped CZA catalysts, which show the highest production of methanol from CO_2 rich syngas. On the other hand, water removal during the SEDMES with the Zr and Ga doped catalysts lead to a high production of CO.

Conflicts of interest

There are no conflicts to declare.

Acknowledgements

This work has been developed in the framework of European H2020 project FLEDGED that has received funding from the European Union's Horizon 2020 Research and Innovation Programme under Grant Agreement No. 727600. Cristina Peinado acknowledges funds from *Programa Garantía Juvenil* 2016 from CAM. We acknowledge support of the publication fee by the CSIC Open Access Publication Support Initiative through its Unit of Information Resources for Research (URICI).

Notes and references

1 K. Alper, K. Tekin, S. Karagöz and A. J. Ragauskas, *Sustainable Energy Fuels*, 2020, **4**, 4390–4414.

2 G. W. Huber, S. Iborra and A. Corma, *Chem. Rev.*, 2006, **106**, 4044–4098.
3 Z. Azizi, M. Rezaeimanesh, T. Tohidian and M. R. Rahimpour, *Chem. Eng. Process.*, 2014, **82**, 150–172.
4 J. Sun, G. Yang, Y. Yoneyama and N. Tsubaki, *ACS Catal.*, 2014, **4**, 3346–3356.
5 A. Molino, V. Larocca, S. Chianese and D. Musmarra, *Energies*, 2018, **11**, 1–31.
6 C. H. Bartholomew and R. J. Farrauto, *Fundamentals of Industrial Catalytic Processes*, John Wiley & Sons, Ltd., 2006.
7 J. Ott, V. Gronemann, F. Pontzen, E. Fiedler, G. Grossmann, D. B. Kersebohm, G. Weiss and C. Witte, *Ullmann's Encycl. Ind. Chem.*, 2012, 1–27.
8 K. Klier, V. Chatikavanij, R. G. Herman and G. W. Simmons, *J. Catal.*, 1982, **74**, 343–360.
9 O. Martin, C. Mondelli, A. Cervellino, D. Ferri, D. Curulla-Ferré and J. Pérez-Ramírez, *Angew. Chem., Int. Ed.*, 2016, **55**, 11031–11036.
10 U. Mondal and G. D. Yadav, *J. CO_2 Util.*, 2019, **32**, 299–320.
11 G. Leonzio, *J. CO_2 Util.*, 2018, **27**, 326–354.
12 S. Allahyari, M. Haghighi, A. Ebadi and H. Qavam Saeedi, *Int. J. Energy Res.*, 2014, **38**, 2030–2043.
13 R. Khoshbin and M. Haghighi, *Catal. Sci. Technol.*, 2014, **4**, 1779–1792.
14 A. Hankin and N. Shah, *Sustainable Energy Fuels*, 2017, **1**, 1541–1556.
15 S. Michailos, S. McCord, V. Sick, G. Stokes and P. Styring, *Energy Convers. Manage.*, 2019, **184**, 262–276.
16 R. Peláez, P. Marín and S. Ordóñez, *Fuel Process. Technol.*, 2017, **168**, 40–49.
17 C. Baltes, S. Vukojević and F. Schüth, *J. Catal.*, 2008, **258**, 334–344.
18 F. Song, Y. Tan, H. Xie, Q. Zhang and Y. Han, *Fuel Process. Technol.*, 2014, **126**, 88–94.
19 D. Mao and X. Guo, *Energy Technol.*, 2014, **2**, 882–888.
20 X. J. Tang, J. H. Fei, Z. Y. Hou, X. M. Zheng and H. Lou, *Energy Fuels*, 2008, **22**, 2877–2884.
21 R. Ladera, E. Finocchio, S. Rojas, J. L. G. Fierro and M. Ojeda, *Catal. Today*, 2012, **192**, 136–143.
22 R. M. Ladera, J. L. G. Fierro, M. Ojeda and S. Rojas, *J. Catal.*, 2014, **312**, 195–203.
23 R. M. Ladera, M. Ojeda, J. L. G. Fierro and S. Rojas, *Catal. Sci. Technol.*, 2015, **5**, 484–491.
24 A. Kornas, M. Śliwa, M. Ruggiero-Mikołajczyk, K. Samson, J. Podobiński, R. Karcz, D. Duraczyńska, D. Rutkowska-Zbik and R. Grabowski, *React. Kinet., Mech. Catal.*, 2020, **130**, 179–194.
25 C. Peinado, D. Liuzzi, R. M. Ladera-Gallardo, M. Retuerto, M. Ojeda, M. A. Peña and S. Rojas, *Sci. Rep.*, 2020, **10**, 8551.
26 A. A. Khassin, T. P. Minyukova and T. M. Yurieva, *Mendeleev Commun.*, 2014, **24**, 67–74.
27 K. C. Waugh, *Catal. Lett.*, 2012, **142**, 1153–1166.
28 J. Yoshihara and C. T. Campbell, *J. Catal.*, 1996, **161**, 776–782.
29 A. Ateka, I. Sierra, J. Ereña, J. Bilbao and A. T. Aguayo, *Fuel Process. Technol.*, 2016, **152**, 34–45.
30 H. Ham, S. W. Baek, C. H. Shin and J. W. Bae, *ACS Catal.*, 2019, **9**, 679–690.
31 M. Muhler, E. Törnqvist, L. P. Nielsen, B. S. Clausen and H. Topsøe, *Catal. Lett.*, 1994, **25**, 1–10.
32 L. C. Grabow and M. Mavrikakis, *ACS Catal.*, 2011, **1**, 365–384.
33 Y. Yang, C. A. Mims, D. H. Mei, C. H. F. Peden and C. T. Campbell, *J. Catal.*, 2013, **298**, 10–17.
34 J. B. Hansen and P. E. Højlund Nielsen, *Handb. Heterog. Catal.*, 2008, 2920–2949.
35 F. Dadgar, R. Myrstad, P. Pfeifer, A. Holmen and H. J. Venvik, *Catal. Today*, 2016, **270**, 76–84.
36 I. Martínez, V. Kulakova, G. Grasa and R. Murillo, *Fuel*, 2020, **259**, 116252.
37 S.-H. Kang, J.-W. Bae, W. Jun, K.-S. Min, S.-L. Song and S.-H. Jeong, US 8623927 B2, 2011, vol. 1, p. 5.
38 R. Ladera, F. J. Pérez-Alonso, J. M. González-Carballo, M. Ojeda, S. Rojas and J. L. G. Fierro, *Appl. Catal., B*, 2013, **142–143**, 241–248.
39 D. Liuzzi, E. Fernandez, S. Perez, E. Ipiñazar, A. Arteche, J. L. G. Fierro, J. L. Viviente, D. A. Pacheco Tanaka and S. Rojas, *Rev. Chem. Eng.*, 2020, 20190067.
40 J. van Kampen, J. Boon, F. van Berkel, J. Vente and M. van Sint Annaland, *Chem. Eng. J.*, 2019, **374**, 1286–1303.
41 J. Terreni, M. Trottmann, T. Franken, A. Heel and A. Borgschulte, *Energy Technol.*, 2019, **7**, 1–9.
42 A. Ateka, M. Sánchez-Contador, J. Ereña, A. T. Aguayo and J. Bilbao, *React. Kinet., Mech. Catal.*, 2018, **124**, 401–418.
43 S. C. Baek, S. H. Kang, J. W. Bae, Y. J. Lee, D. H. Lee and K. Y. Lee, *Energy Fuels*, 2011, **25**, 2438–2443.
44 G. Celik, A. Arinan, A. Bayat, H. O. Ozbelge, T. Dogu and D. Varisli, *Top. Catal.*, 2013, **56**, 1764–1774.
45 I. Iliuta, M. C. Iliuta and F. Larachi, *Chem. Eng. Sci.*, 2011, **66**, 2241–2251.
46 Z. Ravaghi-Ardebili and F. Manenti, *Appl. Energy*, 2015, **145**, 278–294.
47 J. van Kampen, J. Boon, J. Vente and M. van Sint Annaland, *J. CO_2 Util.*, 2020, **37**, 295–308.
48 H.-J. Kim, H. Jung and K.-Y. Lee, *Korean J. Chem. Eng.*, 2001, **18**, 838–841.
49 S. Reßler, M. P. Elsner, C. Dittrich, D. W. Agar, S. Geisler and O. Hinrichsen, in *Integrated Reaction and Separation Operations*, Springer, 2006, pp. 149–190.
50 S. N. Khadzhiev, N. V. Kolesnichenko and N. N. Ezhova, *Pet. Chem.*, 2008, **48**, 325–334.
51 M. Stöcker, *Microporous Mesoporous Mater.*, 1999, **29**, 3–48.
52 T. A. Zepeda, B. Pawelec, A. Infantes-Molina, R. I. Yocupicio, G. Alonso-Núñez, S. Fuentes, J. N. Diaz De León and J. L. G. Fierro, *Fuel*, 2015, **158**, 405–415.
53 W. J. Lee, A. Bordoloi, J. Patel and T. Bhatelia, *Catal. Today*, 2020, **343**, 183–190.
54 M. S. Spencer, *Top. Catal.*, 1999, **8**, 259–266.
55 F. Li, M. Ao, G. H. Pham, J. Sunarso, Y. Chen, J. Liu, K. Wang and S. Liu, *Small*, 2020, **16**, 1906276.
56 M. R. Gogate, *Pet. Sci. Technol.*, 2019, **37**, 671–678.
57 M. Sánchez-Contador, A. Ateka, P. Rodriguez-Vega, J. Bilbao and A. T. Aguayo, *Ind. Eng. Chem. Res.*, 2018, **57**, 1169–1178.